Finally, an intriguing feature of the present fibers is shown in scanning electron microscopy pictures of the fiber cross section. Two different domains can be distinguished: a well-defined core that mostly contains SWNTs and an external shell that is composed of spherical carbon particles (as evidenced by microprobe analysis) (Fig. 4, C and D). These carbon impurities, which originate directly from the raw material, are randomly distributed in the initial ribbons (Fig. 4A). Hence, the separation within the fibers should take place as the fibers are collapsing under capillary forces and water evaporation from the initial ribbons. This particular feature may open a new route for the large-scale purification of SWNTs. Chemical, irradiative, or thermal removal of the external shell could lead directly to purified SWNTs.

Preliminary four-probe electrical measurements gave a resistivity at room temperature of about 0.1 ohm-cm and a nonmetallic behavior when the temperature was decreased. This value, three orders of magnitude greater than that previously reported for SWNTs (*18–21*), has to be taken with caution because of the presence of the external shell of carbon particles.

Research is currently under way to examine the mechanical and electrical properties of the present ribbons and fibers as the full phase space of nanotube type, purity, concentration, flow, and injection conditions is explored. Further studies are also highly desirable to improve the mechanical properties of SWNT fibers, perhaps through chemical or thermal treatments. More generally, the present method may also be suitable for making fibers out of other kinds of dispersed particles. Although it is intrinsically different from more classical techniques used to make microfibers by pulling or drawing viscoelastic fluids (*22*), it can also be easily scaled up for high-volume production (*23*).

**References and Notes**


1. G. Overney, W. Zhong, D. Z. Tomanek, *Phys. D* **27**, 93 (1993).
2. D. H. Robertson, D. W. Brenner, J. W. Mintmire, *Phys. Rev. B.* **45**, 12592 (1992).
3. M. M. J. Treacy, T. W. Ebbesen, J. M. Gibson, *Nature* **381**, 678 (1996).
4. J. P. Salvetat *et al.*, *Phys. Rev. Lett.* **85**, 944 (1999).
5. M. R. Falvo *et al.*, *Nature* **389**, 582 (1997).
6. M. S. Dresselhaus, G. Dresselhaus, P. C. Eklund, *Science of Fullerenes and Carbon Nanotubes* (Academic Press, San Diego, CA, 1996).
7. A. Thess *et al.*, *Science* **273**, 483 (1996).
8. C. Journet *et al.*, *Nature* **388**, 756 (1997).
9. J. Chen *et al.*, *Science* **282**, 95 (1998).
10. A. G. Rinzler *et al.*, *Appl. Phys. A* **67**, 29 (1998).
11. An alternative method for making SWNT fibers has recently been published [H. H. Gommans *et al.*, *J. Appl. Phys.* **88**, 2509 (2000)].
12. R. H. Baughman *et al.*, *Science* **284**, 1340 (1999).
13. R. J. Hunter, *Foundations of Colloid Science*, vol. 1 (Oxford Univ. Press, Oxford, 1989).
14. S. Asakura, F. Oosawa, *J. Chem. Phys.* **22**, 1255 (1954).
15. J. M. Bonard *et al.*, *Adv. Mat.* **9**, 827 (1997).
16. M. Doi, S. F. Edwards, *The Theory of Polymer Dynamics* (Oxford Univ. Press, New York, 1986).
17. S. M. Clarke, A. R. Rennie, P. Convert, *Europhys. Lett.* **35**, 233 (1996).
18. H. Dai, E. W. Wong, C. Lieber, *Science* **272**, 523 (1996).
19. J. E. Fisher *et al.*, *Phys. Rev. B* **55**, R4921 (1997).
20. C. L. Kane *et al.*, *Europhys. Lett.* **41**, 683 (1998).
21. J. Hone *et al.*, *Appl. Phys. Lett.* **77**, 666 (2000).
22. I. W. Donald, *J. Mat. Sci.* **22**, 2661 (1987).
23. P. Poulin, B. Vigolo, A. Pénicaud, C. Coulon, CNRS French Patent 0002272 (2000).


24. We gratefully acknowledge R. Baughman for enthusiastic support of this work, R. Canet for assistance in the conductivity measurements, and M. Alrivie for SEM experiments.

20 July 2000; accepted 10 October 2000


# Change in the Probability for Earthquakes in Southern California Due to the Landers Magnitude 7.3 Earthquake

**Max Wyss[1] and Stefan Wiemer[2]**

**The Landers earthquake in June 1992 redistributed stress in southern California, shutting off the production of small earthquakes in some regions while increasing the seismicity in neighboring regions, up to the present. This earthquake also changed the ratio of small to large events in favor of more small earthquakes within about 100 kilometers of the epicenter. This implies that the probabilistic estimate for future earthquakes in southern California changed because of the Landers earthquake. The location of the strongest increase in probability for large earthquakes in southern California was the volume that subsequently produced the largest slip in the magnitude 7.1 Hector Mine earthquake of October 1999.**

The interdependence of fore-, main-, and aftershocks is self-evident, although the physics of the connecting process is not fully understood. In the months after the event, the 65-km-long rupture of the crust near Landers (*1*) increased the seismicity rate more clearly (*2*) and to larger distances (*3*) than did most mainshocks. The enhanced production of small earthquakes in parts of the volume surrounding the Landers earthquake can be explained by a change in the Coulomb fracture criterion (*4*), which measures the difference between the competing forces that promote and inhibit fracture along preexisting faults (*5*).

We investigated the interdependence between the Landers earthquake and the two largest earthquakes that followed it by 3 hours [near Big Bear with magnitude 6.5 and a rupture length of 20 km (*6*)] and by 7 years [near Hector Mine with magnitude 7.1 and a rupture length of 50 km (*7*)], as well as the sustained decrease and increase of the seismicity rate in neighboring areas of southern California (Fig. 1). In the volumes south of the Hector Mine rupture and north of Big Bear, the production of earthquakes was turned off (dashed lines in Fig. 1) at the time of the Landers earthquake while the production was strongly increased in the volume surrounding the Hector Mine hypocenter and north of Landers (solid lines in Fig. 1). The change of seismicity rates in all four volumes persisted to the end of the data set [1999.7 (decimal year)], which coincides with the time of the Hector Mine earthquake. In three of the examples in Fig. 1, the rate remained approximately constant since the Landers event, whereas it decreased from an exceedingly high to a moderately high level in the Hector Mine volume.

These rate changes are measured by changes in the constant $a$ in the frequency magnitude distribution

$$\log N = a - bM \quad (1)$$

where $N$ is the number of events with magnitude larger or equal to $M$. In addition, we examined the change of the ratio of small to large earthquakes, as measured by the $b$ value in Eq. 1, because constants $a$ and $b$ can be used to estimate by extrapolation the recurrence time $T$ of mainshocks with magnitude $M_{\max}$ by

$$T_L(M_{\max}) = \Delta T / 10^{(a - bM_{\max})} \quad (2)$$

where $\Delta T$ is the period over which the $N$ earthquakes have been observed. The abbreviation L stands for "local," meaning the local value for volumes with a constant radius $r$. The annual local probability $P_L$ per unit area $A$ for the occurrence of an earthquake with $M_{\max}$ is the inverse of $T_L$, divided by $A$

[1]Geophysical Institute, University of Alaska, Fairbanks, AK 99775, USA. E-mail: max@giseis.alaska.edu
[2]Federal Institute of Technology, CH-8093, Zürich, Switzerland. E-mail: stefan@seismo.ifg.ethz.ch

$$P_L(M_{max}) = 1/[T_L(M_{max})A] \quad (3)$$

The estimate of the local earthquake probability, using $P_L$, changes when $a$ and $b$ change. Because $a[N(M \geq 0)]$ is not available, we plot $a'$ instead, the number of events with $M \geq 1.6$, which is the minimum magnitude of complete reporting.

Maps of the change of the parameters $a'$, $b$, and $P_L$ at the time of the Landers earthquake, using the declustered (*8*) earthquake catalog with $M \geq 1.6$ for southern California for the period 1981.0 to 1999.7 (*9*) are shown in Fig. 2. To generate these maps (*10*), we placed a grid with node spacing of 3 km over southern California, sampling the earthquakes during the years before and after Landers within $r = 25$ km of each node. We expressed the change in $a'$ by the $Z$ value (*11*), which is proportional to the significance of the rate change. The change in $b$, $\Delta b$, is mapped only if it is significant above the 95% confidence limit according to the Utsu test (*12*).

To the best of our knowledge, the turning on and off of seismicity at distances of several tens of kilometers from a mainshock and lasting many years has not been mapped in detail before. These rate changes exceed 100% at many locations and are highly significant. The changes are sharp (Fig. 1), coinciding with the occurrence time of the Landers earthquake and lasting until the end of the data set (1999.7).

The pattern of increased and decreased seismicity (Fig. 2B) to a large extent follows the lobes of the advancement and retardation of faulting by the Coulomb fracture criterion (*4, 13*). Rupture on a fault is governed by the shear stress parallel to the fault, which tries to move one side relative to the other, and by the normal stress, which is clamping the fault, preventing it from slipping (*5*). Thus, the redistribution of stress due to the slip on the Landers rupture advances the probability of rupture in some volumes of the crust, whereas it inhibits rupture in neighboring volumes (assuming similar orientations of available faults in the region).

Rate decreases in seismicity are not noticed as readily as increases. By mapping both decreases and increases quantitatively in comparison to the pre-mainshock rate, we established that the pattern of decreases and increases approximately matches that predicted by the Coulomb changes (*13*).

A controversy exists as to whether or not the Coulomb fracture model predicts the advancement or retardation of earthquakes in the source volume of the Hector Mine mainshock (*4, 7, 14*). Depending on the details of the model used, either result can be obtained. We argue that the changes in seismicity rate that we calculated (Fig. 2B) tell us where the probability of a future large earthquake was enhanced and where it was diminished. We propose that the change in seismicity rate is an important constraint that should be used to select the free parameters that go into the Coulomb model (*5*) and that any credible Coulomb model must correctly predict the change of seismicity rate. In the Hector Mine controversy, the change of the $a'$ value shows a node near the southern end of the aftershock zone, with the rupture in a volume of enhanced seismicity (Fig. 2B).

Differences of the ratio of large to small earthquakes, as a function of space or time, contain information about the local state of the crust (*15*). They are measured by changes in the $b$ value (Eq. 1), which is inversely proportional to the mean magnitude $M_{mean}$

$$b = 2.3/(M_{mean} - M_{min}) \quad (4)$$

where $M_{min}$ is the smallest magnitude used in the sample (*16*). Thus, mapping $b$ is equivalent to mapping the mean magnitude of earthquakes.

Strong and persistent temporal changes in mean magnitude ($b$ value) are rare in the high-quality, modern data sets that we have investigated, except during magmatic intrusions beneath volcanoes (*17*). However, the Landers earthquake changed the ratio of small to large earthquakes produced, in favor of small earthquakes in much of southern California (Figs. 3 and 4). On the basis of Utsu's test (*12*), large differences in $b$ ($\Delta b >$ 0.15) can be established by limited numbers of earthquakes ($n \approx 100$ per sample), but in the case of changes where $\Delta b \leq 0.15$, larger numbers ($n \approx 1000$) are required. Such large numbers are now available because small earthquakes have been monitored for decades in southern California. The probability is small that the two samples of earthquakes compared in Fig. 3, A to C, come from the same, indistinguishable population. This can be verified by noticing that, in the declustered data, during the two 5-year periods before and after Landers, about the same number of $M \geq 2.8$ earthquakes occurred, whereas during the second period, ~2000 more events of $M \geq 1.6$ occurred (Fig. 3C). In the clustered data (Fig. 3B), substantially more medium-sized earthquakes were produced before Landers, whereas almost 4000 more small events occurred after it.

The areas where $b$ values increased because of the Landers earthquake are more extensive than those where it decreased (Fig. 2C), so $b$ values are higher on average after the event, as compared to before (Fig. 3D). Most of the increases in $b$ are due to the enhanced production of small earthquakes (Fig. 3C); some of the local decreases are due to the additional production of medium-sized events.

The pattern of $b$-value change differs somewhat at different latitudes (Fig. 4). The volume south of the Landers epicenter (Fig. 4D) shows an increase of $\Delta b = 0.1$ that diminishes with time, but lasts up to the end of the data set. Just north of the Landers epicenter, the change is strongest ($\Delta b = 0.2$), but lasts only ~5 years (Fig. 4C). North of the Landers aftershock zone, the map (Fig. 2C) shows a decrease in $b$, but mixing this volume with the volume to the west yields, on average, a small increase in this latitude band (Fig. 4B). North of latitude 35.6°N, $b$ fluctuates because several *M*5 mainshocks with aftershock sequences followed Landers.

The probability change $\Delta P$, as mapped in Fig. 2D, is calculated on the basis of the local changes in the parameters $a'$ and $b$, assuming that the commonly used estimate of recurrence time (Eq. 3) is valid and can be transformed into a probability by Eq. 2 (*18*). The same grid is used, and $\Delta P(M \geq 5)$ is plotted as the logarithm of the ratio of $P$ before and

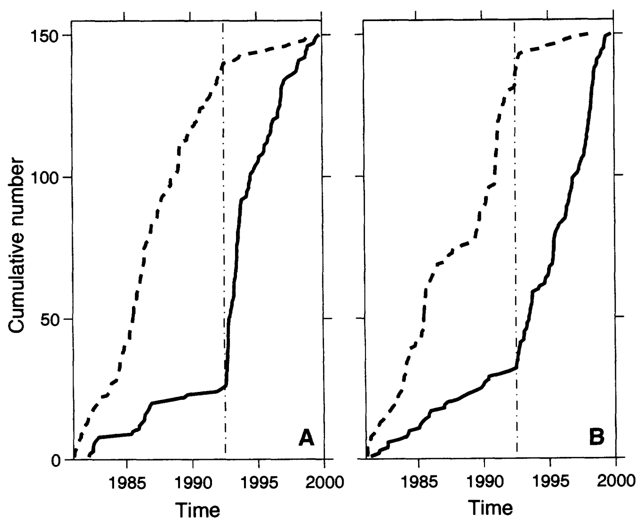


**Fig. 1.** Cumulative numbers of earthquakes ($M \geq 1.6$) as a function of time for four crustal volumes near the Landers earthquake. **(A)** A pair of volumes east of the Landers rupture, one centered at the epicenter of the 1999 *M*7.1 Hector Mine earthquake (solid curve) and one located south of the end of the Hector Mine rupture (dashed curve). **(B)** A pair of volumes west (dashed curve) and north (solid curve) of Landers, in different lobes of the Coulomb fracture criterion change, due to the Landers earthquake. These curves clearly show that profound and lasting seismicity rate changes, with opposite signs in different volumes, occurred at the time of the Landers earthquake.

after the Landers event. Hence, a probability increase of 2 means a 100-fold increase in $P$. In the volume of the Hector Mine mainshock, the increase was nearly 200-fold; at the southern end of that shock, the decrease of $P$ was 3000-fold. The $\Delta P$ for each magnitude bin translates directly into a change in the probabilistic earthquake hazard (for example, the change in the predicted horizontal peak ground acceleration) using standard seismological techniques.

In some volumes, the elevated seismicity rate decreases over the years (Fig. 1A), similar to an aftershock sequence. This, together with the gradual changes in $b$ values (seen for the bulk data in Fig. 4) should change $P$ as a function of time; however, there was little difference in the pattern on maps for $P$ calculated from the seismicity data for 1992.55 to 1993.55, compared to data for 1995 to 1999.7. The general pattern remained the same, with the intensity level of $P$ somewhat decreased in the second period. There are some volumes in which the sign of the probability change switched from the first period to the second. These include (i) the Garlock fault, (ii) the southern part of the Landers rupture with the Palm Springs rupture, and (iii) the northernmost part and the volume to the north of the Hector Mine rupture. We conclude that the imprint of the Landers mainshock on earthquake probability in southern California is lasting and modifies slowly with time (Figs. 1 and 4).

At 70% of the nodes, the sign of the seismicity rate change (Fig. 2B) agrees with the sign of the change in a simple Coulomb failure model that was not adjusted to fit the seismicity data (*13*). This supports the idea that the rate increases and decreases observed after the Landers mainshock (Fig. 1) are due to a static change in the Coulomb failure criterion. By calculating the change of stress at every earthquake location before and after Landers, Gross and Kisslinger (*19*) quantitatively showed a correlation between the stress change and the seismicity for 1.5 years following Landers, to distances of 85 km. Here, we show that the influence included decreases of seismicity rate in some volumes (which lasted to the present) to distances of ~100 km, a distance similar to that found for the increase in precursory moment release (*20*).

The source volume of the Hector Mine earthquake showed the strongest increase in probability (Fig. 2D) but ruptured 7 years after the Landers earthquake, whereas the Big Bear *M*6.5 earthquake ruptured within 2 hours. We propose that this difference lies in the degree of preparation for failure. The Big Bear volume had been in a state of precursory quiescence for 2 years when the Landers earthquake (which was itself preceded by a 4-year quiescence) occurred (*6*). The quiescence hypothesis (*21–24*) suggests that a highly unusual decrease of seismicity rate, without a nearby mainshock, can be a precursor to a mainshock and may indicate that the affected volume is primed for rupture.

Although the estimate of the absolute value of $P$ is not the topic of this report, we estimated it, based on the declustered seismicity since 1993.0, with Eq. 2. The northern part of the source volume of the Hector Mine earthquake does not show the greatest probability, but it ranks in the top 20% of volumes in the study area, excluding the Landers–Big Bear aftershock volumes. Thus, we conclude that our proposed simple calculation of $P$ may be helpful in identifying volumes of increased potential for mainshocks.

The observed changes of seismicity rate suggest the following qualitative model of the crust. We assume that all of southern California, caught between two major tectonic plates, is riddled with small faults. These are zones of weakness and can fail in small to moderate earthquakes. In any given period, some volumes generate many small earthquakes, while others do not, which means that the $a'$ value varies as a function of space (Fig. 3A). We propose that the volumes not producing earthquakes during a given period are not less capable of producing them, but are in a temporary stress shadow and can be activated at any time by a redistribution of stress due to a large earthquake (Figs. 1 and 2B). Conversely, the activity in seismically active volumes can be turned off at any time by the same process (Figs. 1 and 2B). However, the maximum size of the earthquake likely in each volume still depends on the largest well-developed fault in each volume.

The observation of relatively low $b$ values in southern California before the Landers earthquake agrees with the pattern of more medium-sized events before the 1952 *M*7.5

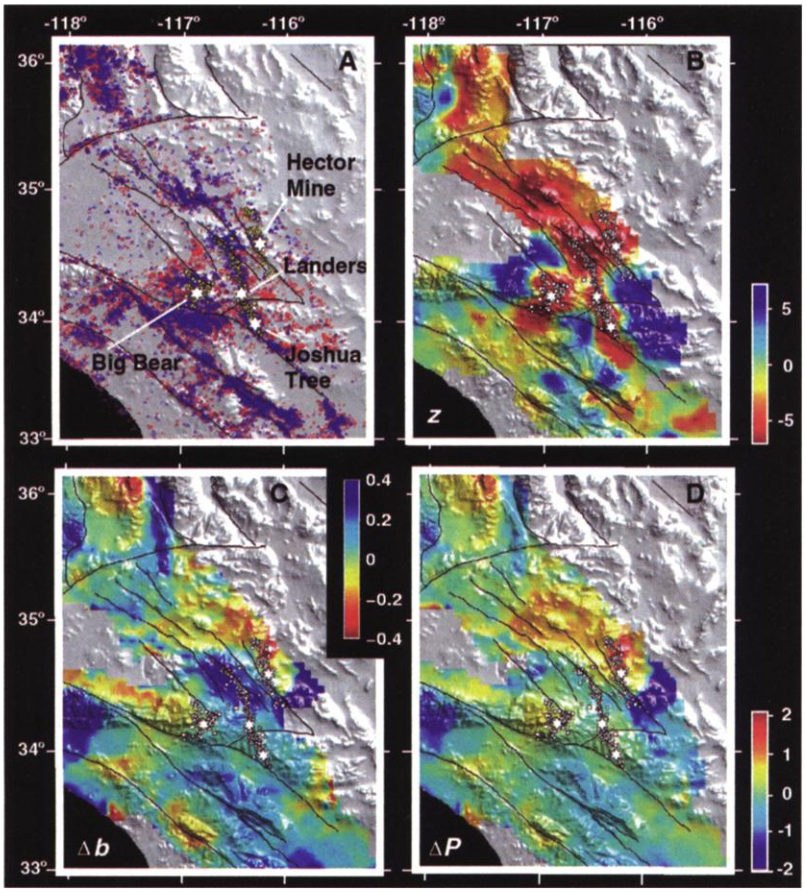


**Fig. 2.** Maps of the changes of the seismicity parameters during the 7 years following the Landers *M*7.3 earthquake compared to the data during the 12.5 years before the event. Yellow circles represent large aftershocks ($M > 3$) of the Landers, Big Bear, and Hector Mine shocks, outlining their source volumes. (**A**) Epicenters of earthquakes with $M \geq 1.6$ for the study period (1981 to 1992.48, red; 1992.48 to 1999.7, blue). (**B**) Rate change of seismicity before and after the Landers mainshock measured by the standard deviate $Z$. (**C**) Change of $b$ value (ratio of small to large earthquakes), comparing the data before and after Landers. Blue areas map locations where $b$ increased (proportionally more small earthquakes) after the Landers earthquake; red areas show decreases of $b$ (relatively more medium-sized earthquakes). (**D**) Change in probability for earthquakes with $M \geq 5$ estimated from the $a$ and $b$ values, comparing the data before and after Landers. These maps were produced by calculating the parameters at each node of a grid, spaced by 3 km, on the basis of the sample of events within 25 km of the node.

Kern County earthquake (*25*) as compared to after it. Furthermore, it agrees with the hypothesis that the moment release increases exponentially as a function of time toward an approaching mainshock (*26–28*).

On the basis of the correlation of high $b$ values with low ambient stress (*29–31*), we tentatively suggest that the Landers earthquake reduced the stress, even in some volumes where the Coulomb criterion increased the probability of failure (*5*), and hence the generation of smaller earthquakes is favored, leading to larger $b$ values. In a low-stress environment, the probability of any rupture growth is reduced. Ruptures that begin in small, highly stressed volumes cannot easily connect to adjacent volumes of locally high stress, because of the energy well that is encountered. In volumes of higher ambient stress, the energy wells are not as deep and, on average, ruptures grow larger. Alternatively, it may be that the crust in southern California contains a fabric of faults, which has different size distributions or different coefficients of friction in different directions. In the first case, a rotation of the acting stress tensor could alter the average rupture length due to the different geometry. In the second case, the average rupture length could be altered because different coefficients of friction may lead to different rupture lengths (*32*). The detailed mapping of locations where earthquake production was decreased will also be important in understanding the processes that dynamically govern the weakening (*33*) or strengthening (*34*) of fault zones, due to the passing of seismic waves.

We observed a strong decrease in $b$, coupled with an increase in $a'$, in the northwestern part of the Hector Mine rupture (Fig. 3C), which leads to the greatest increase in probability at that location (Fig. 3D). This was also the location of the largest moment release along the Hector Mine rupture (*14*). Following the idea that $a'$ and $b$ are both sensitive to stress leads to the conclusion that the change in probability should be a function of the change in stress. This is supported by the pattern of $\Delta P$ (Fig. 3D), which shows positive and negative lobes like the $Z$ value (Fig. 3B) and the Coulomb criterion (*4*, *13*).

We conclude that the 1992 $M7.3$ Landers earthquake turned seismicity production on and off in neighboring volumes by redistributing the stress and that, on average, more small earthquakes were produced after it. These changes of the parameters $a'$ and $b$ lead to 100-fold changes in the probability calculated for mainshocks on the basis of seismicity parameters. The Landers shock triggered one major earthquake immediately (Big Bear $M6.5$ within 2 hours) in a volume that had shown precursory quiescence for 2 years before, and it advanced the probability for another large earthquake (Hector Mine $M7.1$) that occurred 7 years later within the volume of greatest probability change. Therefore, our results quantitatively support the idea that large earthquakes affect the earthquake potential within distances of about twice their source radii (*35–40*) and for durations of decades. Consequently, probabilistic seismic hazard assessment needs to progress from being time-independent (Poissonian) to being time-dependent, by incorporating the probability changes caused by large mainshocks.

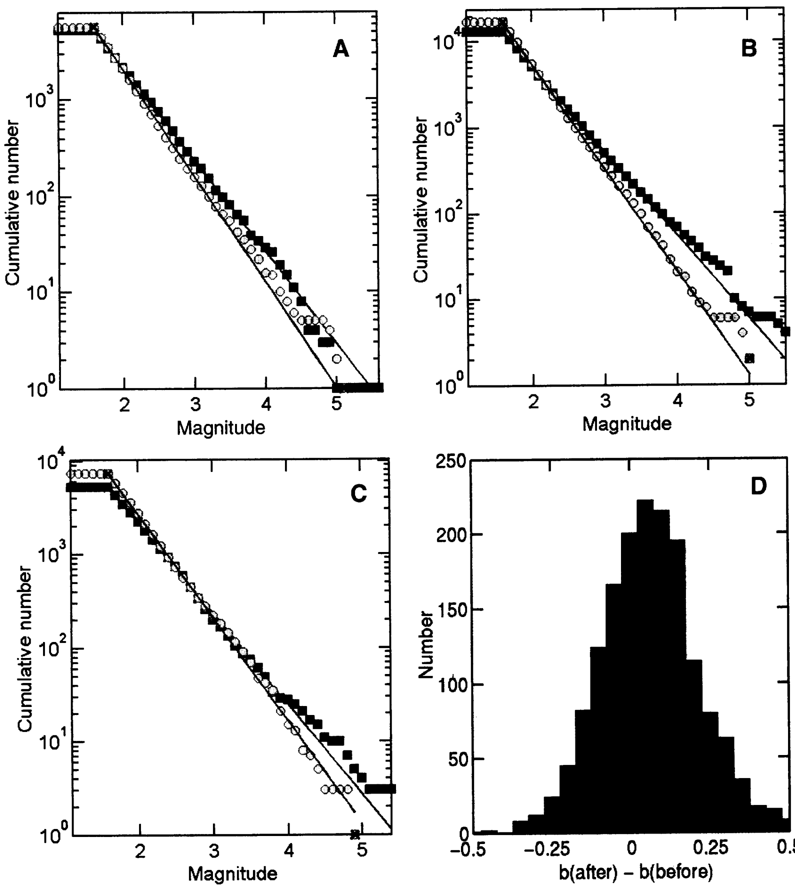


**Fig. 3.** Comparisons of the frequency-magnitude distribution in large regions of southern California before and after the Landers earthquake. (**A**) Declustered (no aftershocks) catalog for a trapezoidal area south of the Landers epicenter, down to and between the Salton Sea and San Diego. Squares, 1981 to 1992.4; circles, 1992.5 to 1999.7. The minimum and maximum magnitudes used are marked by ×. Numbers of events are $n_1 = 5334$ and $n_2 = 5692$, $b$ values before and after are $b_1 = 0.96$ and $b_2 = 1.1$, and the probability that these are indistinguishable samples is $P = 1 \times 10^{-12}$. (**B**) All events (including clusters) south of the Landers epicenter. Squares, 1981 to 1992.4; circles, 1992.5 to 1999.7. $n_1 = 13{,}187$, $n_2 = 16{,}991$, $b_1 = 0.98$, $b_2 = 1.2$, and $P = 1 \times 10^{-72}$. (**C**) Declustered catalog for earthquakes 5 years before and after Landers (1987.2 to 1992.2 and 1992.5 to 1997.5) occurring on land in the study area (Fig. 1A) and south of the northern tip of the Landers rupture. $n_1 = 5235$, $n_2 = 7375$, $b_1 = 0.97$, $b_2 = 1.0$, and $P = 3 \times 10^{-12}$. (**D**) Histogram for changes in $b$ value, calculated for nodes of a grid as used in the map of Fig. 2C.

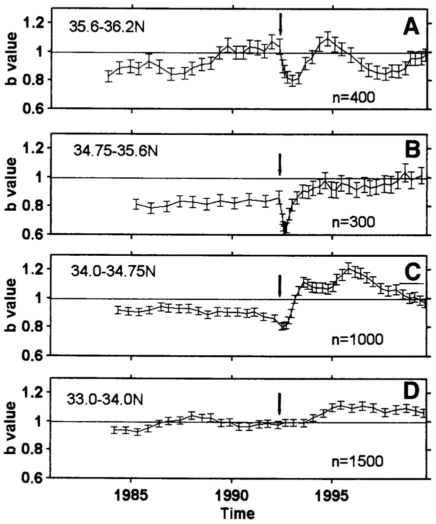


**Fig. 4.** (**A** through **D**) Values of $b$ as a function of time in four segments of latitude in southern California. The number of earthquakes in the sliding time windows and the latitude range are given in each frame. The data set was declustered, and $M \geq 1.6$. The occurrence time of the Landers earthquake is marked by arrows. The brief dip in $b$ is due to more medium-sized events during the aftershock period, a feature common to most aftershock sequences. Error bars indicate 1 SD of the weighted least squares fit.

## References and Notes

1. D. J. Wald, T. H. Heaton, *Bull. Seismol. Soc. Am.* **84**, 668 (1994).
2. D. P. Hill *et al.*, *Science* **260**, 1617 (1993).
3. P. Bodin, J. Gomberg, *Bull. Seismol. Soc. Am.* **84**, 835 (1994).
4. R. S. Stein, G. C. P. King, J. Lin, *Science* **258**, 1328 (1992).
5. The Coulomb failure stress change $\Delta\sigma_f = \Delta\tau - \mu(\Delta\sigma_n - \Delta\Pi)$, where $\Delta\tau$ is the shear stress change resolved into the fault plane, $\Delta\sigma_n$ is the stress change perpendicular to the fault plane (positive toward the plane), $\mu$ is the coefficient of friction, and $\Delta\Pi$ is the pore pressure, measures the change of stress on preexisting faults that is due to a redistribution of stress by a major tectonic event. Increasing $\tau$ or reducing $\sigma_n$ advances the probability of failure. This probability is also increased if a reduction of $\tau$ is accompanied by an even larger reduction in $\sigma_n$. The free parameters of the model are (i) orientation of the local fault plane, (ii) details of the geometry of the main rupture, (iii) orientation of the regional stress field (in the case of choosing planes with optimal orientation), (iv) $\mu$, and (v) $\Pi$. We suggest that these parameters are poorly known, with margins of error that allow adjustments, such that the observed seismicity rate changes are correctly modeled. We view the quantitatively established pattern of increased and decreased seismicity as a solid observation that may help constrain the model along with other data, such as the measurements of surface deformations near the mainshock.
6. S. Wiemer, M. Wyss, *Bull. Seismol. Soc. Am.* **84**, 900 (1994).
7. Scientists from the U.S. Geological Survey, Southern California Earthquake Center, and California Division of Mines and Geology, *Seismol. Res. Lett.* **71**, 11 (2000).
8. The analysis reported was performed on the declustered [P. A. Reasenberg, *J. Geophys. Res.* **90**, 5479 (1985)] data set because the estimate of the background values of $a'$ and $b$ should not be contaminated by aftershocks and swarms. However, we also performed all analyses using the full data set, including aftershocks. We found that the results do not depend on the inclusion or exclusion of clusters.
9. The homogeneity of reporting earthquakes over decades and as a function of space is a thorny question that we have investigated in detail before conducting seismicity studies [F. R. Zuniga, M. Wyss, *Bull. Seismol. Soc. Am.* **85**, 1858 (1995); F. R. Zuniga, S. Wiemer, *Pure Appl. Geophys.* **153**, 713 (1999)]. In general, most reported rate changes are due to artificial causes, and we have developed criteria by which some of these can be identified. We examined the earthquake catalog for southern California (Southern California Earthquake Center) by the GENAS algorithm [R. E. Habermann, *J. Geophys. Res.* **88**, 5056 (1983)] and found that it is of high quality since 1981, but does contain some changes that may be artificial. The changes we report here do not conform to patterns of known artificial changes; they coincide with the time of the Landers earthquake, and they have opposite signs (increase and decrease in neighboring volumes). Therefore, these changes are likely of natural origin. In addition, we deleted small volumes that contained a strong preponderance of daytime events from the analysis, because these are most likely explosions.
10. S. Wiemer, thesis, University of Alaska, Fairbanks (1996).
11. Instead of reporting percentages of rate changes, which could be large but statistically insignificant, we estimate the statistical significance of the rate change at a given time $t_c$ by the standard deviate $Z$ test, $Z = (\mu_2 - \mu_1)/(S_1/n_1 + S_2/n_2)^{1/2}$. The larger the difference between the two means, $\mu$, and the larger the numbers of samples, $n$, before and after $t_c$ (index 1 and 2, respectively), the more confidence one can place in the significance of a difference, whereas large variances of the means, $S$, decrease the confidence.
12. T. Utsu, in *Report of the Joint Research Institute for Statistical Mathematics* (Institute for Statistical Mathematics, Tokyo, 1992), vol. 34, pp. 139–157.
13. D. Marriott, S. Hreinsdottir, M. Wyss, *Eos* **81**, S302 (2000).
14. T. Parsons, D. S. Dreger, *Geophys. Res. Lett.* **27**, 1949 (2000).
15. Recently, we have shown that the $b$ value is not as constant ($b \approx 1$) as previously thought [C. Frohlich, S. Davis, *J. Geophys. Res.* **98**, 631 (1993); Y. Y. Kagan, *Pure Appl. Geophys.* **155**, 537 (1999)] and can vary between 0.5 and 1.5 along fault zones [S. Wiemer, M. Wyss, *J. Geophys. Res.* **102**, 15115 (1997); Y. Ogata, K. Katsura, *Geophys. J. Int.* **113**, 727 (1993); F. Amelung, G. King, *Geophys. Res. Lett.* **24**, 507 (1997)]. We tested the hypothesis that asperities, the crucial hard spots that control main ruptures, may be mapped by minima in $b$ values and in $T_L$ values [M. Wyss, D. Schorlemmer, S. Wiemer, *J. Geophys. Res.* **105**, 7829 (2000)]. Thus, asperities seem to be locations that produce more medium-sized earthquakes, relative to small ones, than does the normal crust.
16. K. Aki, *Bull. Earthquake Res. Inst.* **43**, 237 (1965).
17. Increasingly detailed earthquake catalogs reveal that, beneath volcanoes, volumes surrounding the magma chambers produce far more small earthquakes ($b$ = 1.5) than does the rest of the crust [(*41*); S. Wiemer, S. McNutt, *Geophys. Res. Lett.* **24**, 189 (1997); M. Murru, C. Montuori, M. Wyss, E. Privitera, *Geophys. Res. Lett.* **26**, 2553 (1999)] and that temporal changes of $b$ values occur during intrusions [(*41*); M. Wyss, K. Shimazaki, S. Wiemer, *J. Geophys. Res.* **102**, 20413 (1997)].
18. The seismic hazard is usually expressed in expected ground acceleration, which is calculated on the basis of $P$, using attenuation laws and source zone definitions, as well as long historic earthquake catalogs. In addition, some national efforts of mapping the seismic hazard include information on crustal deformation. On occasion, attempts are made to estimate the time-dependent hazard, by also considering the occurrence time of the last large earthquakes on prominent faults. Here, we focus exclusively on the element of hazard assessment brought in by the turning on and off of seismicity due to stress redistribution by major ruptures.
19. S. J. Gross, C. Kisslinger, *J. Geophys. Res.* **102**, 7603 (1997).
20. D. D. Bowman, G. Ouillon, C. G. Sammis, A. Sornette, D. Sornette, *J. Geophys. Res.* **103**, 24359 (1998).
21. N. Kato, M. Ohtake, T. Hirasawa, *Pure Appl. Geophys.* **150**, 249 (1997).
22. M. Wyss, A. H. Martyrosian, *Geophys. J. Int.* **134**, 329 (1998).
23. M. Wyss, A. Hasegawa, S. Wiemer, N. Umino, *Ann. Geophys.* **42**, 851 (1999).
24. M. Wyss, S. Wiemer, *Pure Appl. Geophys.* **153**, 259 (1999).
25. L. M. Jones, E. Hauksson, *Geophys. Res. Lett.* **24**, 469 (1997).
26. D. J. Varnes, *Pure Appl. Geophys.* **130**, 661 (1989).
27. S. Jaume, L. R. Sykes, *Pure Appl. Geophys.* **155**, 279 (1999).
28. C. G. Sammis, S. W. Smith, *Pure Appl. Geophys.* **155**, 307 (1999).
29. C. H. Scholz, *Bull. Seismol. Soc. Am.* **58**, 399 (1968).
30. M. Wyss, *Geophys. J. R. Astron. Soc.* **31**, 341 (1973).
31. T. I. Urbancic, C. I. Trifu, J. M. Long, R. P. Young, *Pure Appl. Geophys.* **139**, 449 (1992).
32. J. Boatwright, M. Cocco, *J. Geophys. Res.* **101**, 13895 (1996).
33. D. Kilb, J. Gomberg, P. Bodin, *Nature*, in press.
34. E. Richardson, C. Marone, *J. Geophys. Res.* **104**, 28859 (1999).
35. T. Parsons, R. S. Stein, R. W. Simpson, P. A. Reasenberg, *J. Geophys. Res.* **104**, 20183 (1999).
36. R. S. Stein, *Nature* **402**, 605 (1999).
37. P. A. Reasenberg, R. W. Simpson, *U.S. Geol. Surv. Prof. Pap.* **1550-D**, D49 (1997).
38. V. I. Keilis-Borok, L. Knopoff, I. Rotwain, C. R. Allen, *Nature* **335**, 690 (1988).
39. L. Knopoff, T. Levshina, V. I. Keilis-Borok, C. Mattoni, *J. Geophys. Res.* **101**, 5779 (1996).
40. F. Press, C. Allen, *J. Geophys. Res.* **100**, 6421 (1995).
41. S. Wiemer, S. R. McNutt, M. Wyss, *Geophys. J. Int.* **134**, 409 (1998).


42. We thank M. Gerstenberger, C. Sammis, and three anonymous reviewers for comments on the manuscript. This research was supported by NSF grant EAR 9902717. This paper is contribution number 1151 of the Geophysical Institute, Eidgenössische Technische Hochschule, Zürich.

21 July 2000; accepted 4 October 2000


# Sediments at the Top of Earth's Core


**Bruce A. Buffett,[1]* Edward J. Garnero,[2] Raymond Jeanloz[3]**



**Unusual physical properties at the core-mantle boundary have been inferred from seismic and geodetic observations in recent years. We show how both types of observations can be explained by a layer of silicate sediments, which accumulate at the top of the core as Earth cools. Compaction of the sediments expels most of the liquid iron but leaves behind a small amount of core material, which is entrained in mantle convection and may account for the isotopic signatures of core material in some hot spot plumes. Extraction of light elements from the liquid core also enhances the vigor of convection in the core and may increase the power available to the geodynamo.**


The boundary between Earth's liquid iron core and silicate mantle coincides with a region of unusual structural complexity (*1*). Strong lateral variations in $P$- and $S$-wave velocity are evident in the lowermost 200 km of the mantle (*2–5*). More substantial anomalies in the seismic velocities, possibly in excess of $-10\%$ (relative to the average seismic velocities in the lowermost mantle), have been detected within a few tens of kilometers of the core-mantle boundary (CMB) in several regions (*6–9*). These ultralow-velocity zones (ULVZs) have been interpreted as evidence for partial melt (*10*), although alterna-


[1]Department of Earth and Ocean Sciences, University of British Columbia, Vancouver, British Columbia V6T 1Z4, Canada. [2]Department of Geological Sciences, Arizona State University, Tempe, AZ 85287, USA. [3]Department of Earth and Planetary Science, University of California, Berkeley, CA 94720, USA.

*To whom correspondence should be addressed. E-mail: buffet@eos.ubc.ca